

# Melting and Equilibrium Shape of Icosahedral Gold Nanoparticles

Yanting Wang and S. Teitel

*Department of Physics and Astronomy, University of Rochester, Rochester, NY 14627*

Christoph Dellago

*Institute for Experimental Physics, University of Vienna, Boltzmannngasse 5, 1090 Vienna, Austria*

(Dated: February 8, 2020)

We use molecular dynamics simulations to study the melting of gold icosahedral clusters of a few thousand atoms. We pay particular attention to the behavior of surface atoms, and to the equilibrium shape of the cluster. We find that although the surface of the cluster remains ordered up to the melting  $T_m$ , the increasing mobility of vertex and edge atoms significantly soften the surface structure, leading to inter- and intra-layer diffusion, and shrinking of the average facet size, so that the average shape of the cluster is nearly spherical at melting.

PACS numbers: 05.45.-a, 79.60.-I

Keywords: Clusters, gold nanocrystals, molecular dynamics

Gold particles consisting of tens to thousands of atoms have unique optical and mechanical properties and hold great promise as building blocks for nano-bioelectronic devices [1, 2], catalysts [3], and sensors [4]. It is therefore natural that the physics and chemistry of these materials are a current research subject of great interest [5]. For future applications knowledge of the structure and stability of gold nanoparticles of different size and morphology is particularly important.

While bulk gold has an fcc crystal structure, the competition between bulk and surface energies in nanometer sized gold crystallites can result in several different competing structures [6, 7]. Depending on cluster size and external conditions transitions between these structures have been observed [7, 8]. One such structure which has been observed both in simulations [9, 10] and in experiments [11, 12], is the ‘‘Mackay icosahedron’’ [13, 14], consisting of 20 slightly distorted fcc tetrahedra, with four  $\{111\}$  faces each, meeting at the center to form an icosahedral shaped cluster. The internal faces of the tetrahedra meet at strain inducing twin grain boundaries with hcp structure, leaving the cluster with 20 external  $\{111\}$  facets. Theoretical models [15, 16, 17] have predicted different limits for the stability of such icosahedral clusters, and it is unclear whether their formation is an equilibrium or rather a kinetic process [11, 16, 17, 18, 19, 20]. Nevertheless, it is natural to suppose that formation of this structure is related to the very high stability of the  $\{111\}$  external surfaces. Simulations [21] and experiments [22] on bulk slab-like geometries with exposed  $\{111\}$  surfaces have shown that, unlike the  $\{100\}$  and  $\{110\}$  surfaces which melt below the bulk melting temperature  $T_m$ , the  $\{111\}$  surface neither melts nor roughens but remains ordered up to and above  $T_m$ , and can in fact lead to superheating of the solid [23]. In light

of this observation it is interesting to consider how the high stability of the  $\{111\}$  facets effects the melting and equilibrium shape of such icosahedral nanoclusters.

In order to address this issue, we have performed detailed numerical simulations of gold nanoclusters of a few thousand atoms, paying particular attention to the behavior of the surface atoms and to the equilibrium shape. We find that there is a considerable softening of the cluster surface roughly  $\sim 200$  K below  $T_m$  due to the motion of atoms along the vertices and edges of the cluster. In this region we find both intra-layer and inter-layer diffusion of atoms, which increases considerably as  $T_m$  is approached. The equilibrium shape progresses from fully faceted, to faceted with rounded edges, to nearly spherical just below  $T_m$ . Throughout this region, the interior atoms of the cluster remain essentially perfectly ordered, until  $T_m$  is reached.

Using the many-body ‘‘glue’’ potential [24] to model interactions among gold atoms, we carry out molecular dynamics simulations, integrating the classical equations of motion with the velocity Verlet algorithm [25] with a time step of 4.3 fs. The results presented here are for a 2624 atom cluster, of size  $\sim 20$  Å, but we have also considered other sizes. We start our simulations at a high  $T = 1500$  K  $> T_m$ , and cool using the Andersen thermostat method [25] to 1000 K. We then cool, in intervals of 100 K, down to 200 K, using  $5 \times 10^6$  steps (21 ns) at each temperature. The cluster structure we find with this method is an almost perfect Mackay icosahedron, but with a missing central atom. Such a central vacancy, postulated for copper and aluminum but not for gold [26], has been considered previously [27] as a means of partially relieving the strain caused by the hcp twin grain boundaries between the fcc tetrahedra.

To study melting and the equilibrium shape, we next

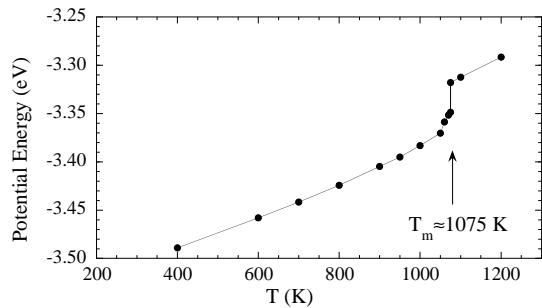


FIG. 1: Potential energy vs.  $T$  for a 2624 atom gold cluster. The sharp jump at  $T = 1075$  K indicates the first order melting transition.

heat the cluster up using constant temperature molecular dynamics[28]. To compute equilibrium properties, we take at each temperature  $10^6$  steps (4.3 ns) for equilibration, followed by  $10^7$  steps (43 ns) to compute averages. We take fine temperature increments in the vicinity of the cluster melting transition. In Fig. 1 we show our results for the average potential energy vs. temperature. We found the cluster to melt at  $T_m = 1075$  K, with a discontinuous jump in potential energy.

To characterize the structure of the cluster, we measure the standard bond orientational order parameters  $Q_6$ ,  $\hat{W}_6$ ,  $Q_4$  and  $\hat{W}_4$  [29]. To distinguish between bulk and surface behavior, we first identify all atoms on the surface of the cluster, then the atoms in the first sub layer below the surface, and so on; the cluster has 9 such layers. We label as “interior” atoms those lying below the fourth sub layer. In Fig. 2a we plot the bond order parameters averaged over only bonds between the interior atoms. We see  $Q_4$ ,  $\hat{W}_4 \approx 0$  at all  $T$ , while  $Q_6$  and  $\hat{W}_6$  take finite values for  $T < T_m$  appropriate to the Mackay icosahedron.  $Q_6$  and  $\hat{W}_6$  remain essentially constant, decreasing only slightly just below  $T_m$ , indicating that the bulk ordering remain stable up until melting. In contrast, Fig. 2b shows the bond order parameters averaged over only bonds between the surface atoms. Again  $Q_4$ ,  $\hat{W}_4 \approx 0$  at all  $T$ , while  $Q_6$  and  $\hat{W}_6$  take finite values for  $T < T_m$ . However here we see a much more pronounced decrease, particularly in  $Q_6$  starting well below  $T_m$ , until both vanish at melting (the finite value of  $Q_6$  above melting is a finite size effect that decreases as the cluster size increases). Thus, while the surface remains ordered below  $T_m$ , i.e.  $|Q_6|, |\hat{W}_6| > 0$ , the surface order softens to a much greater extent than does the bulk as  $T_m$  is approached.

Next we consider the diffusion of the surface atoms. In Fig. 3a we plot, for several different temperatures, the average mean square displacement  $\langle |\Delta \mathbf{r}(t)|^2 \rangle \equiv \langle |\mathbf{r}(t) - \mathbf{r}(0)|^2 \rangle$  vs. time  $t$ , where the average is over all the atoms which were initially on the surface of the cluster. At  $T = 600$  K, diffusion is negligible, with displacements on

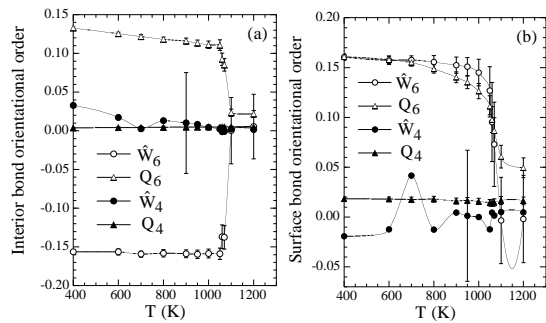


FIG. 2: Bond orientational order parameters,  $Q_6$ ,  $\hat{W}_6$ ,  $Q_4$ ,  $\hat{W}_4$  vs.  $T$ , averaged over (a) bonds between interior atoms only, and (b) bonds between surface atoms only. For  $\hat{W}_4$  only a few representative error bars are shown for the sake of clarity.

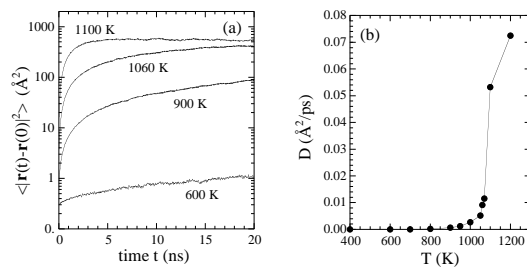


FIG. 3: (a) Mean square displacement for atoms initially on the surface, at various temperatures; (b) Diffusion constant  $D$  vs.  $T$  for atoms initially on the surface.

the order of one atomic separation. At  $T = 900$  K, almost 200 K below  $T_m$ , diffusion is significant. At  $T = 1060$  K, 15 K below  $T_m$ , the mean square displacement saturates at large  $t$ , indicating that atoms now diffuse the entire length of the cluster. Fitting the early time linear part of these curves,  $\langle |\Delta \mathbf{r}(t)|^2 \rangle \sim 6Dt$ , we plot the diffusion constant in Fig. 3b.

The question thus arises how to reconcile this observed surface diffusion below  $T_m$  with the absence of surface melting that is indicated by the finite bond orientation order parameters of Fig. 2b. Our answer is given by the last row of figures shown in Fig. 4. For each atom initially on the surface of the cluster, we compute its average position  $\bar{\mathbf{r}} \equiv \langle \mathbf{r} \rangle$ , and its average displacement correlation matrix  $d_{\alpha\beta} \equiv \langle (r - \bar{r})_\alpha (r - \bar{r})_\beta \rangle$ , where  $\alpha, \beta = x, y, z$  and the  $\langle \dots \rangle$  stand for averages over 25 configurations, sampled every 43 ps of simulation time. Taking the eigenvectors of  $d_{\alpha\beta}$  and the square root of their corresponding eigenvalues to define the axes and principal radii of an ellipsoid, gives a convenient representation for the root mean square displacement of the atom. In the last row of Fig. 4 we plot these ellipsoids for each atom initially on the surface, centering the ellipsoid at the average position of the atom  $\bar{\mathbf{r}}$ . We show such plots for the same temperatures as in Fig. 3a. We clearly see that for  $T = 600$  K and

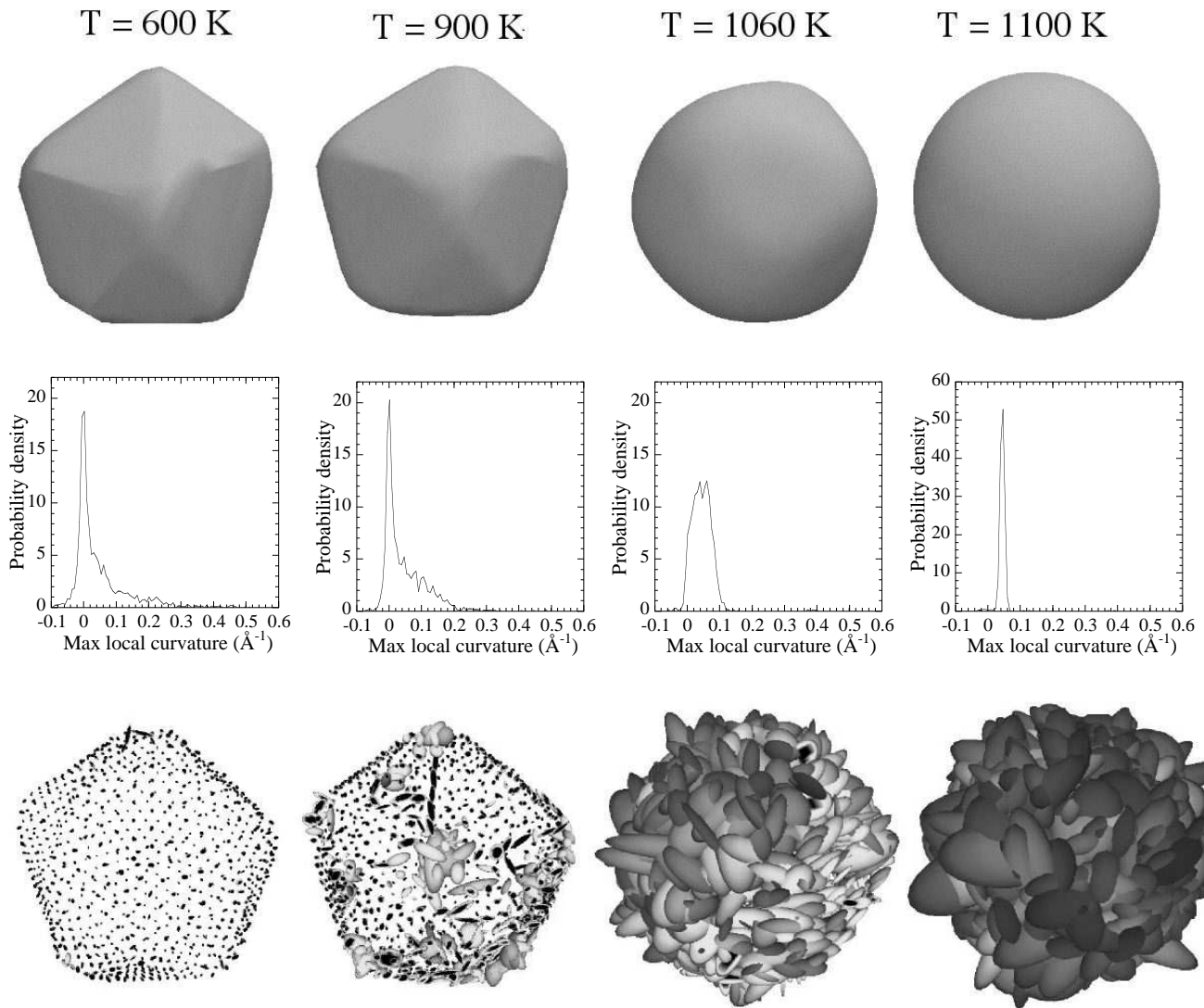


FIG. 4: For the indicated temperatures, top row: average cluster shape for a simulation time of 43 ns; middle row: histogram of the maximal local curvatures of the average shape; bottom row: ellipsoids indicate root mean square displacements of atoms on the cluster surface over a simulation time of 1.075 ns.

900 K, the biggest ellipsoids are at the vertices and edges, while those for atoms in the facets are in general smaller. If we let the time that we average over increase, we find that the ellipsoids at the vertices and edges grow in size, corresponding to diffusion, while those in the middle of the facets stay approximately the same, corresponding to thermal vibrations without diffusion. A more detailed analysis shows that significant interlayer exchange takes place between the two topmost layers as much as 200 K below  $T_m$ . In Fig. 4 one can see ellipsoids oriented normal to the cluster surface, corresponding to this interlayer diffusion. For the higher temperatures,  $T = 1060$  K just below melting, and  $T = 1100$  K just above melting, diffusion is pronounced throughout the entire surface.

Finally, we consider the effects of the vertex and edge

atom diffusion on the equilibrium shape of the cluster. Because of the small cluster size, the instantaneous shapes fluctuate significantly at high temperatures. But since our simulation algorithm conserves angular momentum, and the angular momentum is zero, our sample does not rotate as a whole, and hence there is a well defined average equilibrium shape at each temperature. We measure this equilibrium shape by averaging over the instantaneous shapes as follows. We divide space up into 842 approximately equal solid angles [30], corresponding roughly to the number of surface atoms. We then average the position of the surface atoms found in each solid angle over 1000 configurations sampled at equal times throughout the simulation of total time 43 ns. This defines the average radial position of the cluster within each solid

angle, and hence the average cluster shape. In the top row of Fig. 4 we show the resulting equilibrium shapes for several temperatures. We see that the shape is rounding out as the temperature increases, assuming a nearly perfect spherical shape above  $T_m$ .

To quantify this, we compute the curvature distribution of the surface as follows. Using the average position of the surface in a given solid angle and its nearest neighbors, we fit to determine the best tangent plane to these points. Defining the normal to this plane as the  $z$  axis, we then find the best paraboloid that fits through the points. The principal curvatures of this paraboloid then give our approximation for the two principal curvatures of the surface at the given solid angle. We define  $\kappa$  to be the maximum of these two principal curvatures. In the middle row of Fig. 4 we plot histograms of  $\kappa$  as one varies over all the solid angles defining the average surface. At  $T = 600$  K and 900 K we see a sharp peak at  $\kappa = 0$  corresponding to the points on flat facets, and a high  $\kappa$  tail corresponding to higher curvatures on the edges and vertices. At  $T = 1060$  K, just below  $T_m = 1075$  K, the peak at  $\kappa = 0$  has essentially vanished, and one has a broad distribution centered about  $\kappa \simeq 1/R$  with  $R = 21.5$  Å, the radius of the spherical liquid drop above  $T_m$ . At  $T = 1100$  K, just above  $T_m$ , the distribution becomes very sharply peaked about  $\kappa = 1/R$ .

To conclude, we have found that gold nanoparticles of a few thousand atoms form a Mackay icosahedral structure, with missing central atom, when cooled from a liquid. Upon slow heating, we find that this bulk structure remains stable up to melting. The surface stays ordered, however softens considerably with increasing diffusion due to mobile vertex and edge atoms. As  $T_m$  is approached, this diffusion of edge atoms leads to significant shrinkage of the  $\{111\}$  facet sizes in the average cluster shape, leading to an almost spherical shape just below  $T_m$ . In addition to the cluster of 2624 atoms reported upon here, we have also considered clusters of different sizes from 1409 to 5082 particles. While the melting temperature  $T_m$  was observed to increase with increasing cluster size, we continued to find the same general features, with the surface softening tracking the increase in  $T_m$ . It would be interesting to know how this surface softening is related to morphological transitions observed in gold nanorods at temperatures below the melting temperature [28, 31].

This work was funded in part by DOE grant DE-FG02-89ER14017.

---

[1] M. G. Warner and J. E. Hutchison, *Nature Materials* **2**, 272 (2003).  
 [2] Y. Xiao, F. Patolsky, E. Katz, J. F. Hainfeld, and I.

Willner, *Science* **299**, 1877 (2003).  
 [3] A. T. Bell, *Science* **299**, 1688 (2003).  
 [4] S. O. Obare, R. E. Hollowell, and C. J. Murphy, *Langmuir* **18**, 10407 (2002).  
 [5] *Metal Nanoparticles; Synthesis, Characterization, and Applications*, ed. D. L. Feldheim and C. A. Foss, Dekker, New York (2002).  
 [6] S. Iijima and T. Ichihashi, *Phys. Rev. Lett.* **56**, 616 (1986).  
 [7] C. L. Cleveland, W. D. Luedke, and U. Landman, *Phys. Rev. B* **60**, 5065 (1999).  
 [8] L. J. Lewis, P. Jensen, and J.-L. Barrat, *Phys. Rev. B* **56**, 2248 (1997).  
 [9] Y. G. Chushak and L. S. Bartell, *J. Phys. Chem. B* **105**, 11605 (2001).  
 [10] H.-S. Nam, Nong M. Hwang, B. D. Yu, and J.-K. Yoon, *Phys. Rev. Lett.* **89**, 275502 (2002).  
 [11] L. D. Marks, *Rep. Prog. Phys.* **57**, 603 (1994).  
 [12] J. A. Ascencio, C. Gutiérrez-Wing, M. E. Espinosa, M. Martín, S. Tehuacanero, C. Zorrilla, and M. José-Yacamán *Surf. Sci.* **396**, 349 (1998).  
 [13] A. L. Mackay, *Acta Cryst.* **15**, 916 (1962).  
 [14] T. P. Martin, *Phys. Rep.* **273**, 199 (1996).  
 [15] G. Wulff, *Z. f. Kristallog.* **34**, 449 (1901); C. Herring, *Phys. Rev.* **82**, 87 (1931).  
 [16] S. Ino, *J. Phys. Soc. Japan* **27**, 941 (1969).  
 [17] C. L. Cleveland, U. Landman, M. N. Shafiqullin, P. W. Stephens, and R. L. Whetten, *Z. Phys. D* **40**, 503 (1997).  
 [18] C. L. Cleveland, U. Landman, T. G. Schaaff, M. N. Shafiqullin, P. W. Stephens, and R. L. Whetten, *Phys. Rev. Lett.* **79**, 1873 (1997).  
 [19] K. Michaelian, N. Rendon, and I. L. Garzon, *Phys. Rev. B* **60**, 2000 (1999).  
 [20] L. D. Marks, *Phil. Mag.* **49**, 81 (1984).  
 [21] P. Carnevali, F. Ercolessi, and E. Tosatti, *Phys. Rev. B* **36**, 6701 (1987).  
 [22] K. D. Stock and B. Grosser, *J. Cryst. Growth* **50**, 485 (1980).  
 [23] F. D. Di Tolla, E. Tosatti, and F. Ercolessi, in *Monte Carlo and Molecular Dynamics of Condensed Matter Systems*, K. Binder and G. Ciccotti (Eds.), Società Italiana di Fisica, Bologna, 1996, p. 345-398.  
 [24] F. Ercolessi, M. Parrinello, and E. Tosatti, *Philos. Mag.* **A58**, 213 (1988).  
 [25] D. Frenkel and B. Smit, *Understanding Molecular Simulation*, Academic Press, 2nd ed. (2002).  
 [26] C. Mottet, G. Treglia, and B. Legrand, *Surf. Sci.* **383**, L719 (1997).  
 [27] L. L. Boyer and J. Q. Broughton, *Phys. Rev. B* **42**, 11461 (1990).  
 [28] Y. Wang and C. Dellago, *J. Phys. Chem. B* **107**, 9214 (2003).  
 [29] P. J. Steinhardt, D. R. Nelson, and M. Ronchetti, *Phys. Rev. B* **28**, 784 (1983).  
 [30] R. H. Hardin, N. J. A. Sloane and W. D. Smith, *Tables of Spherical Codes with Icosahedral Symmetry*, published electronically at <http://www.research.att.com/~njas/icosahedral.codes/>.  
 [31] S. Link, Z. L. Wang, and M. A. El-Sayed, *J. Phys. Chem. B* **104**, 7867 (2000).